

Cover letter

Dear Editor

Please see below a combined file including

- 1) response letter
- 2) revised manuscript

The response letter was given in such a format that the comments are text in black colour and our responses are given in red text.

The revised manuscript has considered all comments from reviewers. The changes are those text marked with yellow background.

Thank you for considering our manuscript to be published on ESSD.

Best regards,

Bin Cheng and co-authors.

Comments from first reviewer and responses from the authors

The paper as submitted represents a significant effort to measure and analyse long-term trends in Boreal Lake ice behaviours and the results are very relevant to ongoing monitoring of climate changes. The paper also details useful developments in the instrumentation used and the methods of analysis of the data the instruments produce.

This reviewer is an Engineer involved in the initial development of the instrumentation used and cannot comment on the metrological and climatological issues raised and analysed. Comments are limited to instrumentation matters only.

The work details a considerable programme of over a decade duration over which the SIMBA instrument has developed. The authors present advances made in the instrument itself and improved methods of deployment but more significantly is the presentation of results from a newly developed algorithm to process the SIMBA data. This is a major advancement in the use of the SIMBA device as to date the interpretation of results has been largely subjective human activity. The use of this algorithm now allows for a repeatable and consistent analysis of the considerable data set collected.

Specific comments on the text are as follows.

The SIMBA sensors are calibrated at a single point to remove large offsets in a very accurately controlled bath. The sensors have been shown to be very linear and so the largest source of error becomes the resolution of the sensors. The absolute accuracy is therefore in the region of the resolution plus the error in the water bath accuracy which is very small. The quoted $\pm 0.01\text{C}$ is not possible and the accuracy more like $\pm 0.0625\text{C}$. The sensor drift over time is small and can largely be ignored.

Reply: Thank you to point out this error. We made correction accordingly. The new text read: The accuracy of the SIMBA thermistor sensor is $\pm 0.1\text{ }^{\circ}\text{C}$, which is comparable with other type of thermistor string based IMBs (Richter-Menge et al. 2006).

Diffusivity is a transient measure of how heat is conducted away when a temperature change occurs (i.e. how cold to the touch something is). The SIMBA heating cycle is usually long enough for the temperature rise at the sensor to reach a steady state so is it not the thermal conductivity which dominates?

Reply: We modified the text to: The SIMBA heating cycle is usually long enough, often 60 or 90 s, for the temperature rise at the sensor to reach a steady state. Thermal conductivity determined how the heat is conducted away of the heated sensors placed in air, snow, ice and lake water. As a result, the SIMBA-HT profiles can greatly enhance the detection of the interfaces between air, snow, ice and water.

Really impressive plots!

Reply: Thanks

Overall this is a paper worthy of publication and represents an impressive and well executed effort at studying important phenomena.

Thank you for your positive comment on this work, we appreciate your great effort making this novel, compact and cost cutting instrument, which allow us to carry out sustainable field campaigns.

Comments from second reviewer and responses from the authors

This paper used a thermistor string-based snow and ice mass balance apparatus (SIMBA), which is a novel monitoring method for snow and ice thickness, to monitor the temperatures of air, snow, ice and water, and to get the snow and ice products applying a algorithm, finally to reveal the relationship between climate change and snow/ice thickness. Based on the decadal date sets, authors described the snow and ice temperature regimes, snow depth, ice thickness, and ice compositions as well as meteorological variables at the Finnish Space Centre. These decadal data sets provided firstly can also be used for numerical and satellite validation and can be comparable to the results obtained from other cold regions. So, it is important and interesting issue and is worthy of publication after some revisions. Some comments are raised as follows.

The paper is wrote well entirely. However, there are still some problems in English writing. Such as, “thermal heat conductivity” is suggested to be “thermal conductivity”; Please check “Figure 8” in Line 195 and “Figure 9” in Line 211. It is suggested to revise the English description entirely.

Reply: Thanks for your suggestions. We made corresponding corrections and the language of the entire manuscript has been checked carefully.

“Figure 8” in Line 195 should be “Figure3”
corrected

“Figure 9” in Line 211 should be “Figure4”
corrected

“thermal heat conductivity” in Line 194 modified to “thermal conductivity”
Done

In Lines 328-329, author described “...a decrease of FDD is expected to result in less formation of columnar ice”. Please explain why.

To be more precise, in the revised manuscript, we change FDD and TDD to AFDD and ATDD, respectively. So AFDD is the accumulated freezing degree day, and ATDD is the accumulated thawing degree day. So FDD is a measure of how cold the day is and AFDD is a quantitative estimation on how cold a winter is. Based on classical Stefan’s law (1891), i.e., ice growth is proportional to the accumulated freezing degree day (AFDD). A decrease of AFDD means the winter is less cold, so the columnar ice (ice frozen due to freezing of lake water) is reduced. To avoid confusion, we updated the figure caption: Figure 11. The seasonal accumulated negative freezing degree day (AFDD) and positive thaw degree day (ATDD) during the observation period (2009/2010 – 2019/2020).

In Lines 381-383, the increase of air temperature in winter season is highly correlated with seasonal total accumulated precipitation. Please address its reasons.

In Scandinavia, warm winter weather is typically associated with higher precipitation rates. This is because they are due the same reason. Transient cyclones transport warm, moist air masses to Scandinavia. Without transient cyclones, colder and drier winter weather would prevail in the region. We added two sentences in the conclusion to emphasis this important issue.

In Lines 388-390, the seasonal accumulated FDD is reducing, suggesting reduced formation of columnar ice and, hence, a smaller role of air temperature in controlling the ice thickness. It is a little partial. In cold regions, air temperature is still the dominant factor controlling the ice thickness. Maybe other factor, such as precipitation in winter, play an important role in ice thickening. Please offer the accurate description.

The original description was not very accurate. We were meant to say that the role of air temperature on lake ice formation is getting smaller (because the general warming trend of air temperature in the polar region) rather than the role of air temperature is small. The air temperature is still the number one factor affect ice formation. So, the new sentence is:

Because of the air temperature increase, the seasonal AFDD reduces. This results in a decreasing impact of below-zero air temperatures on lake ice growth during the freezing season, as the growth of columnar ice is reduced. Simultaneously, the role of precipitation on total ice formation is enhanced because snow-ice and superimposed ice contribute to an increasing fraction of the total ice thickness.

1 **Inter-annual variation of lake ice composition in European Arctic: observations based on high-**
2 **resolution thermistor strings**

3
4 Bin Cheng^{1*}, Yubing Cheng^{2,3,1*}, Timo Vihma¹, Anna Kontu¹, Fei Zheng², Juha Lemmetyinen^{1,5},
5 Yubao Qiu^{4,5} and Jouni Pulliainen¹

6 ¹ Finnish Meteorological Institute (FMI), Finland

7 ² Institute of Atmospheric Physics, Chinese Academy of Sciences, Beijing, China

8 ³ University of Chinese Academy of Sciences, Beijing, China

9 ⁴ Aerospace information Research Institute (AIR), Chinese Academy of Science, Beijing China

10 ⁵ FMI-AIR, Joint Research Center for Arctic Observations, Sodankylä, Finland.

11 *corresponding authors:

12 Bin Cheng (bin.cheng@fmi.fi)

13 Yubing Cheng (chengyubing@mail.iap.ac.cn)

14
15 Abstract

16 Climate change and global warming strongly impact the cryosphere. The rise of air temperature and
17 change of precipitation patterns lead to dramatic responses of snow and ice heat and mass balance.
18 Sustainable field observations on lake air-snow-ice-water temperature regime have been carried out
19 in Lake Orajärvi in the vicinity of the Finnish Space Centre, a Flagship Supersite in Sodankylä in
20 Finnish Lapland since 2009. A thermistor string-based snow and ice mass balance buoy called “Snow
21 and ice mass balance apparatus (SIMBA)” was deployed in the lake at the beginning of each ice
22 season. In this paper, we describe snow and ice temperature regimes, snow depth, ice thickness, and
23 ice compositions retrieved from SIMBA observations as well as meteorological variables based on
24 high-quality observations at the Finnish Space Centre. Ice thickness in Lake Orajärvi showed an
25 increasing trend. During the decade of data collection: 1) The November-May mean air temperature
26 had an increasing trend of 0.16° C/year, and the interannual variations were highly correlated ($r =$
27 0.93) with the total seasonal accumulated precipitation; 2) The maximum granular ice thickness

28 ranged from 15 to 80% of the maximum total ice thickness; 3) The snow depth on lake ice was not
29 correlated ($r = 0.21$) with the total precipitation. The data set can be applied to investigate the lake ice
30 surface heat balance and the role of snow on lake ice mass balance, and to improve the
31 parameterization of snow to ice transformation in snow/ice models. The data are archived at
32 <https://zenodo.org/record/4559368#.YIKOOpAzZPZ> (Cheng et al., 2021)

33

34 **1. Introduction**

35

36 The rapid climate warming in the Arctic (Box et al., 2019; Przybylak and Wyszyński, 2020) has also
37 affected lakes, in particular lake surface temperatures and lake ice phenology (Woolway, et al., 2019).
38 In the Northern Hemisphere, the lake ice season has become shorter and lake ice has become thinner,
39 and these trends are projected to continue throughout the 21st century (Sharma, et al., 2019). Lakes
40 are important in the Earth system, as they can adjust local climate (Brown and Duguay, 2010), and
41 affect the environment through interactions among physical, hydrological, biological, and chemical
42 processes (Leppäranta, 2010).

43 Observations on snow depth and lake ice thickness are needed for (a) monitoring of climate variability
44 and trends (Filazzola et al., 2020), (b) practical applications, such as use of lake ice for winter fishing,
45 transport, and recreational activities (Leppäranta, 2015), and (c) to provide initial conditions for
46 operational forecasting (Anderson et al., 2018). Snow depth and lake ice thickness can be measured
47 manually. For example, in Finland, lake ice thickness is measured via manual drilling in a single
48 location in 45 lakes with ten-day intervals throughout the ice season. However, this requires a lot of
49 manpower, and accordingly does not allow collection of time series with a better spatial and temporal
50 resolution. During recent decades, the number manual observations has strongly declined in many
51 countries (Duguay et al., 2006). Satellite remote sensing yields information on lake ice cover (Wu et
52 al., 2021) and snow/ice surface temperature (Cheng et al., 2014) with a sufficiently high spatial and
53 temporal resolution. Kang et al., (2014) introduced a method to derive lake ice thickness from coarse
54 resolution (~ 10 km) passive microwave data over large lakes in Canada. However, the transferability
55 of the method to sub-pixel scale lakes has not been investigated. SAR polarimetry has shown some
56 promise in retrieving ice depth over rivers (Mermoz et al., 2013); as fully polarimetric data is not to

57 date widely available from existing SAR sensors extensive testing and application of the method for
58 lakes is currently lacking.

59 The SIMBA data set is potentially highly relevant for the development of land applications for
60 planned and existing passive microwave satellite sensors, such as the Copernicus Imaging Microwave
61 Radiometer (CIMR), new Metop multichannel radiometer sensors of EUMETSAT, ESA SMOS,
62 NASA SMAP and Chinese sensors. Due to the inherent coarse resolution of these sensors (tens of
63 kilometers), a key issue is to acquire combined simultaneous data representing various processes in
64 lakes, in addition to surrounding land areas. As such, the SIMBA forms an integral part of the FMI
65 sensor network in Sodankylä.

66 Thermistor sting-based snow and ice mass balance apparatus (SIMBA) have been applied for more
67 than a decade to measure snow depth, ice thickness and temperature profile from air through snow
68 and ice to water (Jackson et al., 2013). Most of SIMBA have so far been deployed in Polar sea ice
69 (Lei et al., 2018), but also lake ice has been studied (Cheng et al., 2014; Wei et al., 2016). In this
70 paper we describe SIMBA observations from an ongoing program that started in Lake Orajärvi in
71 northern Finland in 2009. Supporting meteorological observations from Finnish Meteorological
72 Institute Arctic Research Centre (FMI-ARC) are also presented. The objectives of the SIMBA
73 program were

- 74 - to evaluate the cost-effectiveness of SIMBA buoys in a remote lake environment
- 75 - to monitor climate variability and change as reflected in snow depth as well as lake ice
76 thickness and composition
- 77 - to investigate (a) atmospheric forcing on lake ice growth and melt, (b) the role of snow on
78 lake ice mass balance via formation of superimposed ice due to refreezing of melt water
79 and rain and formation of snow ice due to flooding under a heavy snow load, and (c) the
80 role of granular ice in lake ice phenology
- 81 - to develop better parameterizations of snow-to-ice transformation in numerical snow/ice
82 models.

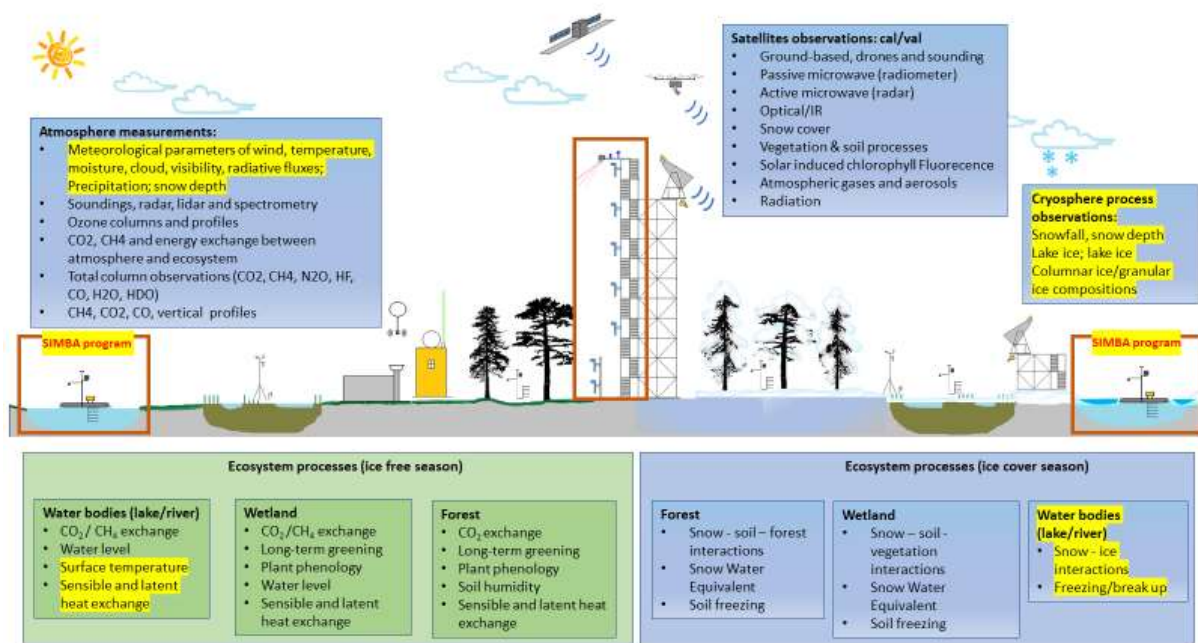
83

84 **2 Observation**

85 **2.1 Sodankylä supersite**

86 The SIMBA program at Lake Orajärvi is a component of the FMI Sodankylä supersite. The Finnish

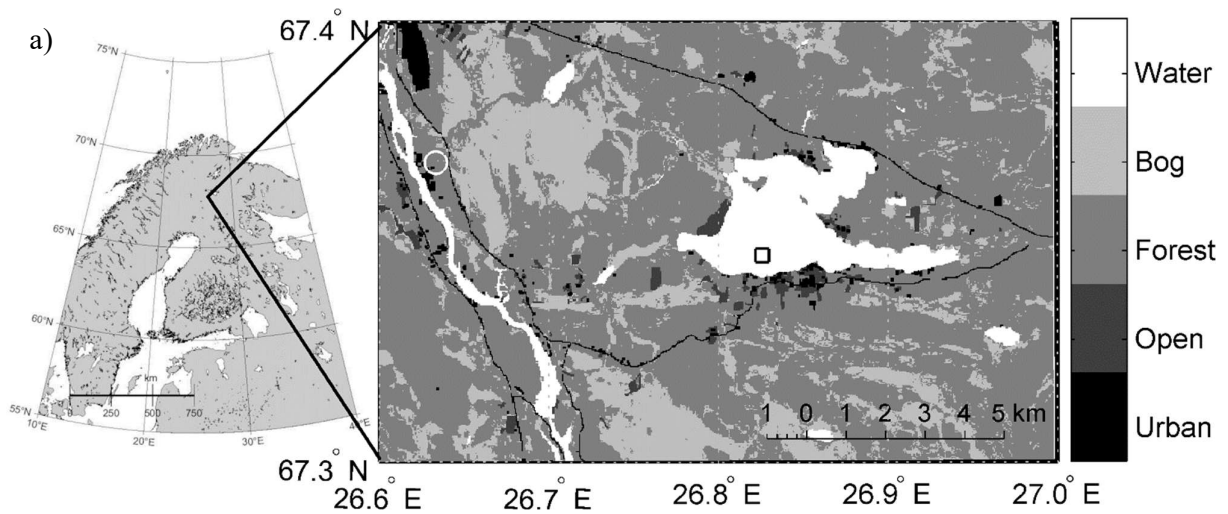
87 Meteorological Institute’s Arctic Space Centre (FMI-ARC) in Sodankylä (67.367 °N, 26.629 °E),
 88 Finland, is a super-observation site where various Earth observations (upper-air chemistry and
 89 physics, atmospheric column measurements, snow and soil hydrology, biosphere-atmosphere
 90 interaction) and ground truth measurements for satellite calibration-validation are carried out
 91 continuously (Fig.1). The site is equipped with comprehensive in situ and remote sensing
 92 instrumentation placed in the forests, wetlands and freshwater bodies, which are the main landcover
 93 types in the area. In this paper we focus on the cryospheric *in situ* observations of snow cover and
 94 lake ice as well as meteorological parameters.



95
 96 Figure 1. Schematic diagram of the FMI-ARC supersite observational systems at Sodankylä. The
 97 original diagram is at <https://litdb.fmi.fi/>. The frames in red and text with yellow background
 98 describes the measurements addressed in this paper.

99
 100 The sub-Arctic climate and the geographic location between continental and marine climate zones
 101 result in a high inter-annual, seasonal and synoptic-scale variation in local weather conditions,
 102 enabling development of very different kinds of snowpack structures on land (Tikkanen, 2005) and
 103 snow/ice composition on lakes (Cheng et al., 2014). Lake Orajärvi is a boreal medium-sized lake
 104 located in Sodankylä municipality in the in the eastern Lapland. The lake has a surface area of about
 105 11 km² with an average depth of 4.4 m and a maximum depth of 11 m close to the southern shore of

106 the lake (Fig. 2a). The estimated water volume in the lake is 0.0485 km^3 , and the shore length is 28
 107 km. The lake surface elevation is 182 m above sea level. The ice season typically starts in November
 108 and lasts until May. The first snowfall typically occurs in late October, but the snow may melt during
 109 warmer autumn days. The seasonally permanent winter snow accumulation usually starts between
 110 mid-November and early-December. Snow is present on the lake ice surface every winter season.
 111



112



113

114

115 Figure 2. a) The location of Lak Orajärvi in Finnish Lapland and a map of lake Orajärvi and local
 116 catchment, where the open black square marks the SIMBA site and white circle is the Finnish Space

117 Centre. b) Snapshots of SIMBA deployment in Lake Orajärvi and a weather station at FMI-ARC
 118 main camp. A raft was anchored in the lake in October 2019 aiming to extend the lake observations
 119 beyond the ice season.

120

121 2.2 SIMBA

122 2.2.1 SIMBA program

123 SIMBA buoys have been deployed in Lake Orajärvi since 2009. The 2009 deployment was probably
 124 the internationally first SIMBA application for a lake study. In each winter when ice was formed in
 125 Lake Orajärvi, one SIMBA was deployed around mid-December at the same site, 67.35° N, 26.83° E,
 126 some 500 m from the shoreline. At the time of deployment, the snow depth, lake ice thickness and
 127 ice freeboard were measured. A supporting frame made of fiberglass was constructed on lake ice, and
 128 the SIMBA main control Peli case was placed on top of it (Fig. 2b). A separate wooden pole with
 129 scale was standing vertically to hold the thermistor string. An ice borehole was drilled through the ice
 130 layer, and the thermistor string was placed in it. The scene was left as it is, and then the thermistor
 131 string was frozen with surrounding water in the borehole. The SIMBA operated in the lake over the
 132 winter and most of the spring melting season. The recovery of SIMBA took place usually in late April
 133 but in some years as late as mid-May. Snow and ice conditions around the deployment site were
 134 documented and measured before dismantling the SIMBA camp. The documentation on SIMBA
 135 deployment and recovery is provided along with the SIMBA data as online files (see data availability).
 136 Table 1 summarizes the SIMBA deployment and recovery status.

137

138 Table 1. SIMBA deployment and recovery days and simultaneous manually observed snow depth (h_s),
 139 total ice thickness (H_i), and ice freeboard (H_{fb} , defined as negative if the lake water level was above
 140 the snow/ice interface) The seasonal mean values were derived from SIMBA-ET and SIMBA-HT
 141 observations. H_{gi} is the granular ice and H_{ci} is the congelation ice thickness.

Season	Deployment				Recovery					Seasonal mean \pm STD				
	Date	h_s	H_i	H_{fb}	Date	h_s	H_{ci}	H_i	H_{fb}	H_i	h_s	H_{sfb}	H_{gi}	H_{ci}
	DD/MM/YY	(cm)			DD/MM/YY	(cm)								
2009/2010	16/12/09	5	27	0	07/04/10	31	54	64	5	NA				
2010/2011	SIMBA was not deployed; only manual observations every second week were available.													

2011/2012	19/12/2011	16	14	-4	12/04/2012	24	22	55	-3	38±16	22±6	5±2	15±10	23±7
2012/2013	12/12/2012	18	33	+1	25/04/2013	0	39	59	6	57±7	26±7	-5±3	4±4	53±4
2013/2014	12/12/2013	14	27	+1	30/04/2014	20	35	35	-3	49±7	17±4	-3±2	10±2	40±6
2014/2015	14/12/2014	19	30	-2.5	23/04/2015	2	35	69	4	54±11	24±7	-4±3	16±8	38±4
2015/2016	18/12/2015	18	27	-1	22/04/2016	5	30	71	6	60±16	19±7	-2±3	12±9	48±9
2016/2017	16/12/2016	8	31	-1	24/04/2017	10	38	72	4	58±13	19±6	-1±2	6±8	50±8
2017/2018	15/12/2017	25	23	-9	03/05/2018	0	28	55	6	48±15	24±6	-4±3	27±14	21±3
2018/2019	13/12/2018	15	19	-2	02/05/2019	1	20	55	6	51±17	21±7	-1±3	21±14	30±7
2019/2020	03/10/2019	-			12/05/2020	4	13	68	7	49±24	24±9	-1±3	32±20	20±5

142 The seasonal mean values of H_i , h_s , H_{gi} , and H_{ci} were calculated by the SIMBA algorithm (Cheng et al., 2020). The
143 seasonal mean value of ice freeboard (H_{sfb}) was calculated based on time series of snow depth (h_s), granular ice thickness
144 (H_{gi}) and columnar ice thickness (H_i) according to the Archimedes' principle: $H_{sfb} = H_i + H_{gi} - (h_s\rho_s + H_{gi}\rho_{gi} +$
145 $H_i\rho_i)/\rho_w$, where ρ_s , ρ_{gi} , ρ_i and ρ_w are seasonal mean densities of snow, granular-ice and columnar ice and lake water,
146 assumed to be 320 kg/m³, 890 kg/m³ and 910 kg/m³ and 1000 kg/m³, respectively. The STD is the standard deviation.

147

148 2.2.2 SIMBA buoy

149 SIMBA is a thermistor string-based Snow and Ice Mass Balance Apparatus. It has been developed
150 by the Scottish Association for Marine Science (SAMS) Research Services Ltd (SRSL) in UK.
151 SIMBA consists of a simple, robust thermistor string with 240 temperature sensors distributed evenly
152 (2 cm intervals) along a 4.8 m long heat-shrink PVC plastic sleeve coated flat white wire. White heat-
153 shrink sleeve is used to minimize the possibility of solar heating of the sensors. The accuracy of the
154 SIMBA thermistor sensor is ± 0.1 °C, which is comparable with other type of thermistor string based
155 IMBs (Richter-Menge et al. 2006). Each sensor measures the environment temperature (SIMBA-ET).
156 The resolution of the thermistor sensor is 0.0625°C, i.e., smaller changes cannot be detected even if
157 the absolute accuracy of the sensor would allow it. In addition, the thermistor chain is equipped with
158 heaters, i.e. resistor components mounted next to the temperature-sensing elements. A weak voltage
159 (8 V) supply is connected to provide gentle identical heating of each sensor on the chain. The SIMBA
160 heating cycle is usually long enough, often 60 or 90 s, for the temperature rise at the sensor to reach
161 a steady state. Thermal conductivity determines how the heat is conducted away of the heated sensors
162 placed in air, snow, ice and lake water. As a result, the SIMBA-HT profiles can greatly enhance the

163 detection of the interfaces between air, snow, ice and water. The heating cycle is applied once per
164 day. The SIMBA-HT is controlled not to disturb the SIMBA-ET measurements which are carried out
165 typically 4 times per day (Jackson et al., 2013). A SIMBA also includes a built-in GPS to record
166 SIMBA drift positions (for sea ice applications), a magnetometer for tilt and floe rotation, a barometer
167 for surface air pressure, and an external sensor to measure near-surface ambient air temperature. An
168 iridium modem is applied for data transmission. SIMBA has been used in various field campaigns
169 targeting snow and ice mass balance in seasonally ice-covers in lakes (Cheng et al., 2014) and Polar
170 Oceans (Hoppmann et al. 2015; Provost et al. 2017; Lei et al. 2018, 2021). Table 1 presents a summary
171 of SIMBA observations in Lake Orajärvi.

172

173 **2.3 Weather station**

174 Meteorological data were collected at FMI-ARC station (67.3666°N, 26.6290°E, WMO code 02836)
175 11 km from Lake Orajärvi. The data sets include wind speed (Va), air temperature (Ta), relative
176 humidity (RH), cloudiness (cn), longwave (Ql) and shortwave (Qs) radiation, snow depth on land (Hs)
177 and precipitation ($Prec$) (Table 2). The radiative fluxes were measured on a 10-m high tower above
178 treetops using Kipp&Zonen CM11 pyranometers (305-2800 nm) and Kipp&Zonen CG4
179 pyrgeometers (4500 - 42000 nm). Snow depth (Campbell Scientific SR50) and precipitation (OTT
180 Pluvio2) at ground level were also measured. All measurements were taken once a minute and
181 aggregated to 1-hour time intervals.

182

183 **3 Data description**

184 **3.1 SIMBA data**

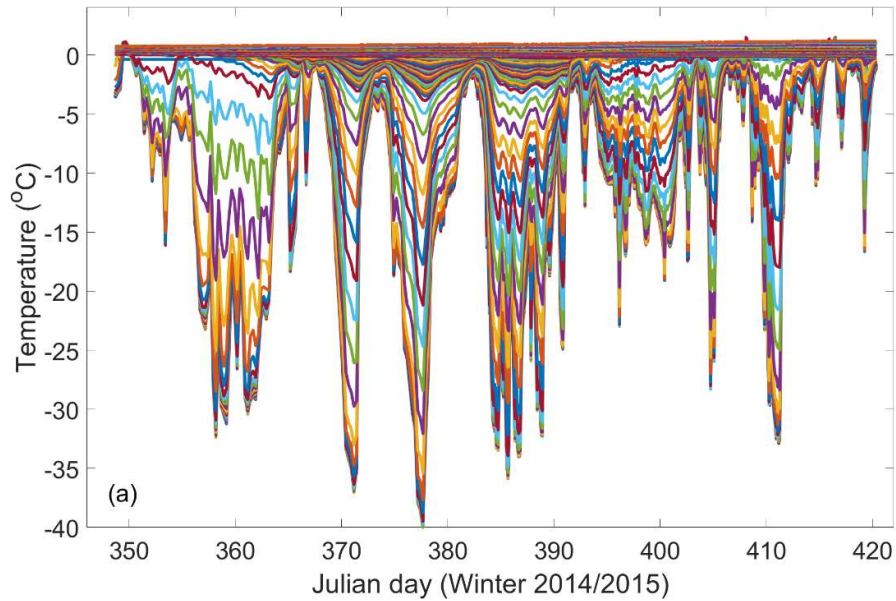
185 The main output of a SIMBA buoy is the time series of environment (SIMBA-ET) and heating
186 (SIMBA-HT) temperature measured at different depths from the lake water through ice and snow to
187 air.

188

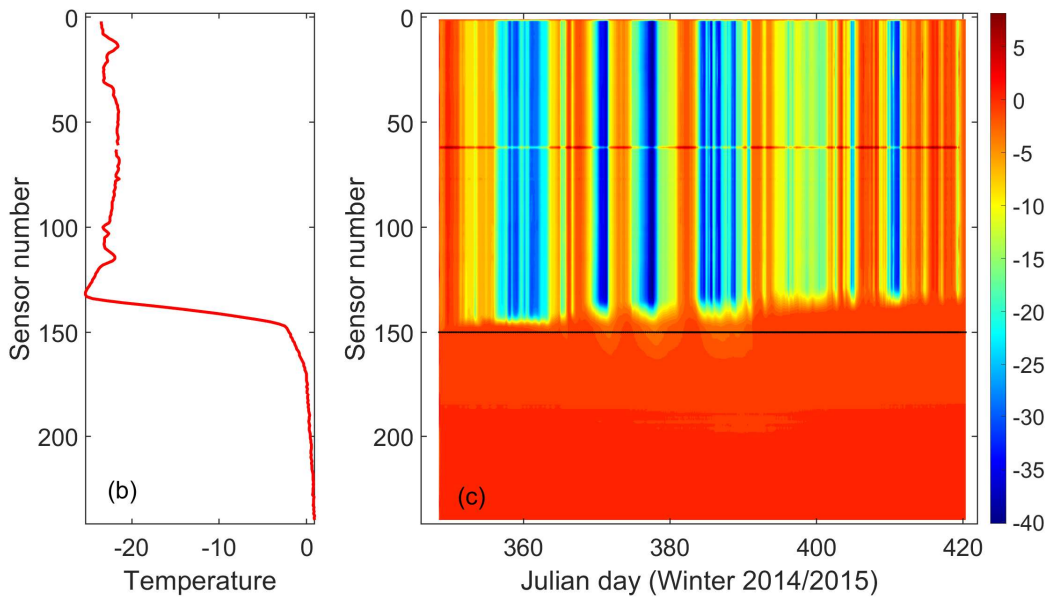
189 *3.1.1 SIMBA-ET*

190 For each season, we have up to 241 time series of temperature (SIMBA-ET) at different depths. For
191 those sensors located in the air, the temperature differences between the sensors are small, as the air
192 in the lowermost 1.5 m layer mixes effectively and the sensors are close to each other. The

193 temperatures inside snow reveal much larger vertical gradients because snow has a small thermal
194 conductivity. The temperature profile in ice has smaller vertical gradient compared to that in snow,
195 since the thermal conductivity of ice is larger than that of snow. At the ice bottom, temperature is at
196 the freezing point and gradually increases towards the lake bottom. Figure 3 shows an example of
197 seasonal SIMBA-ET. One can estimate the heat fluxes within snow and ice, and those at the air-snow,
198 snow-ice, and ice-water interfaces.



199



200

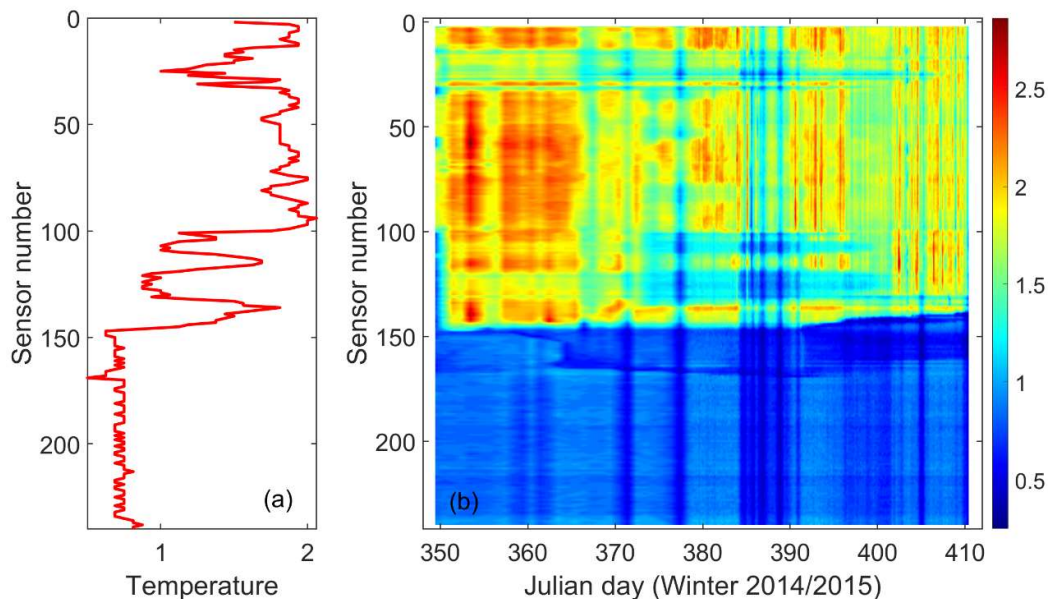
201 Figure 3. Illustrations of SIMBA-ET data: a) Time series of SIMBA-ET during observation period;

202 b) One snapshot (19 Jan 2014 08:00 UTC) of vertical SIMBA-ET profile through air-snow-lake ice-
203 water; c) SIMBA-ET field observed by 240 sensors. Sensor 1 was placed in air and sensor 240 in
204 water.

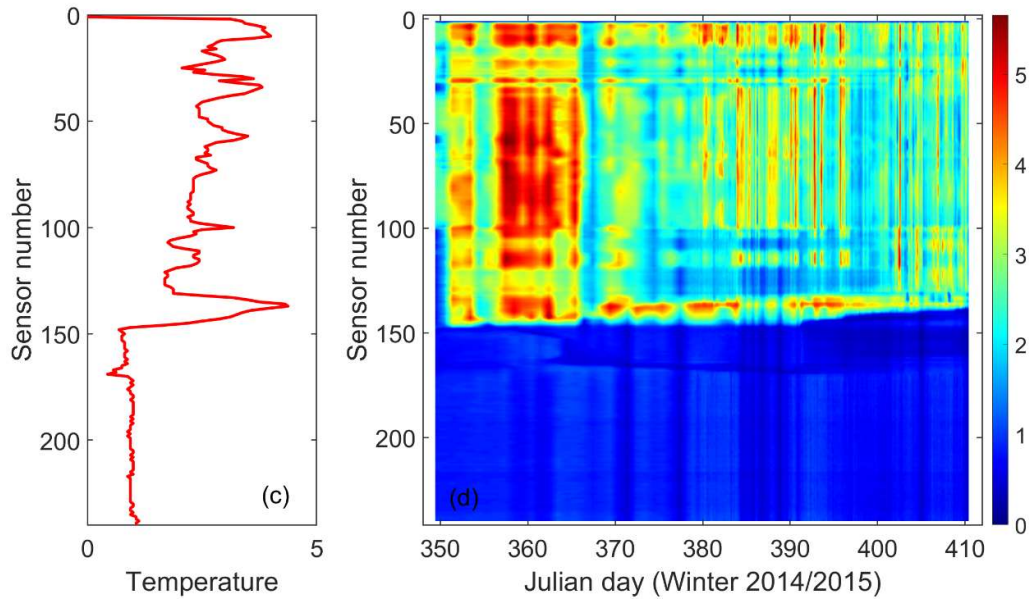
205

206 3.1.2 SIMBA-HT

207 SIMBA-HT shows the temperature increase in the medium each sensor was contacted during a short
208 heating period of 60 s and 90 s. The temperature changes are largely dependent on the thermal
209 diffusivity of the surrounding medium. Low heating power ensures that the temperature increasing
210 will not be too high to melt snow and ice in contact with the sensor and guarantee a fast restore of
211 environment temperature around the sensor before the next SIMBA-ET observation, and above all to
212 minimize SIMBA power consumption. One example of SIMBA-HT is given in Figure 4.



213



214

215 Figure 4. Illustrations of SIMBA-HT: a) a snapshot (25 January, 2015, 18:00 UTC) of vertical profile
 216 of observed temperature increase after 60 s., b) SIMBA-HT (60s) field observed by 240 sensors; c)
 217 Same as a) but after heating for 90 s., and d) SIMBA-HT (90s) field observed by 240 sensors;

218

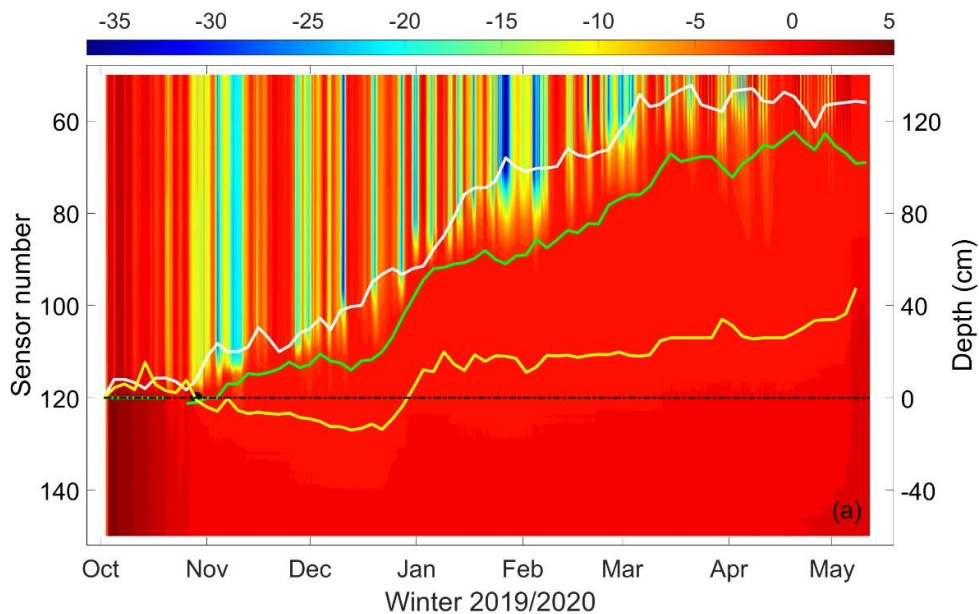
219 3.1.3 SIMBA snow depth and ice thickness

220 Snow depth and ice thickness are derived from SIMBA-ET and SIMBA-HT data. A common
 221 procedure is to look SIMBA-ET temperature profiles manually and identify sudden changes of
 222 vertical temperature gradient to locate the air-snow, snow-ice and ice-water interfaces. The snow
 223 depth is then calculated as the distance between the air-snow and snow-ice interfaces, and the ice
 224 thickness is the distance between the snow-ice and ice-water interfaces. However, a manual procedure
 225 is a heavy task, especially if SIMBA operation covers long period or one would need real time SIMBA
 226 results. Several studies have been carried out aiming development of an algorithm to obtain snow
 227 depth and ice thickness automatically (Liao et al., 2019, Zuo, et al., 2019, Cheng et al., 2020).

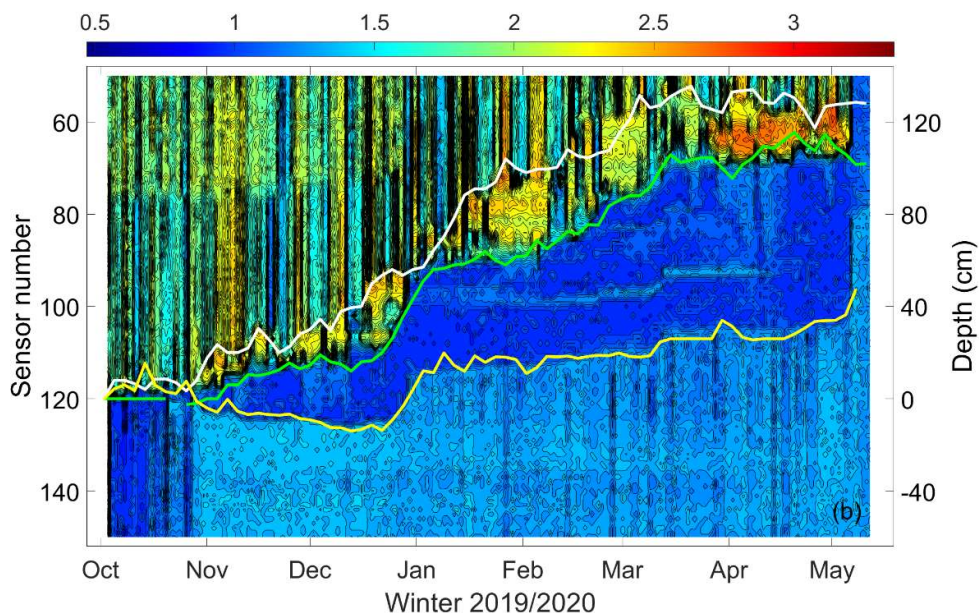
228 Below we present an example of the application of the Cheng et al, (2020) algorithm to retrieve snow
 229 depth and ice thickness from SIMBA data observed in Lake Orajärvi. When SIMBA was deployed,
 230 the initial sensor position at snow-ice interface is known and we defined it as Z_{gi0} , i.e. zero reference
 231 position for granular ice. During observation period, in case if initial snow-ice interface is moving
 232 upward from Z_{gi0} , which is a common phenomenon in Arctic lakes, the distance between Z_{gi0} and
 233 moving snow-ice interface is the new granular ice thickness formed by snow to ice transformation.

234 The depth difference between total ice thickness and granular ice thickness is the congelation ice
235 formed at the ice bottom. Figure 5 shows the air-snow, snow-ice and ice-water interfaces with
236 SIMBA-ET (a) and SIMBA-HT (b) as the background. For better clarity, 5-day running average can
237 be produced as the final products.

238



239



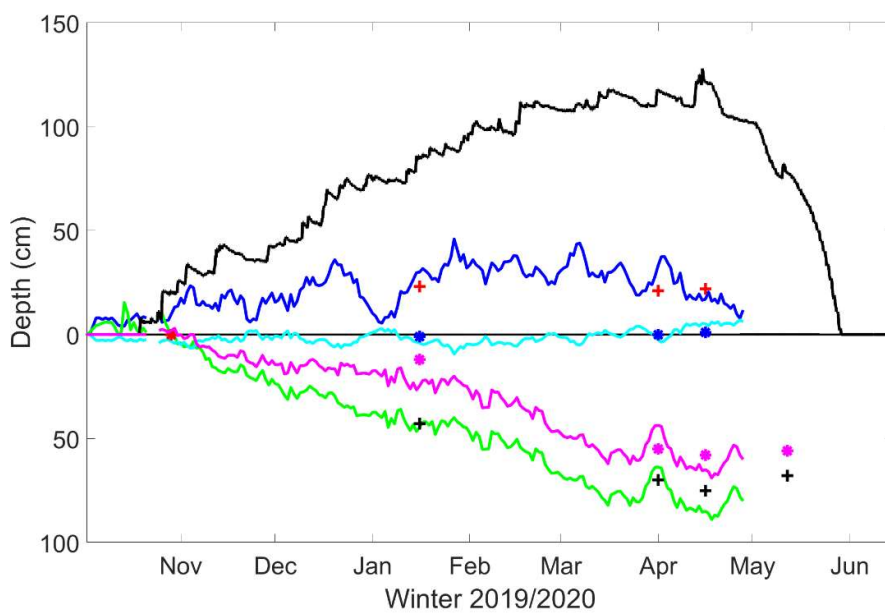
240

241 Figure 5. Time series of sensor position for the air-snow (white), snow-ice (green) and ice-water
242 (yellow) interfaces, identified applying the SIMBA algorithm. The SIMBA-ET observation is

243 illustrated as background in a), and SIMBA-HT ratio (HT60/HT90) in b). The black dash line shows
244 the sensor number (120) at the initial ice surface (Z_{gi0}). For clarity, we only illustrate sensors 50 –
245 150.

246

247 Using snow/ice interface as the zero-reference level, time series can be calculated for the snow depth,
248 snow-ice thickness, total ice thicknesses, and ice freeboard. Figure 6 is an example of the 2019/2020
249 time series, indicating that the lake ice was mainly granular ice, which was related to heavy snow fall
250 during the ice season (the snow depth observed at FMI-ARC weather station on land was highest in
251 a decade).



252

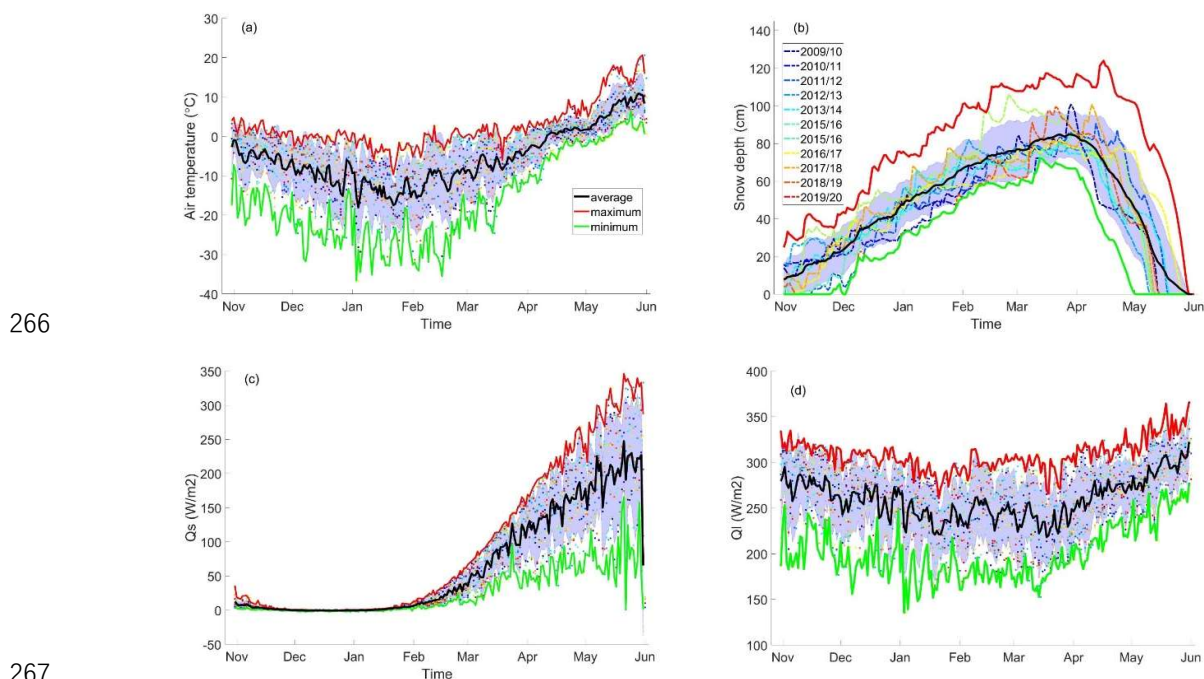
253 Figure 6. Products derived on the basis of SIMBA data: snow depth (blue), ice freeboard (cyan),
254 granular ice thickness (magenta), and total ice thickness (green). The symbols represent manual
255 observations of snow depth (+), ice freeboard (•), granular ice thickness (•) and total ice thickness
256 (+). The black solid line denotes the snow depth on land.

257

258 3.2 Weather data

259 The observed daily mean values of meteorological parameters for all seasons are presented in Figure
260 7. The inter-annual mean, maximum and minimum air temperatures are -2.5°C , -16.5°C and -5.5°C ,
261 respectively. The air temperature reveals a constant decreasing pattern from November to January.
262 The coldest months are January and February. From March onward, the air temperature increased

263 gradually due to increasing solar radiation (Fig. 7c). The inter-annual average, maximum and
 264 minimum downward longwave radiative fluxes are 259 W/m², 309 W/m², and 201 W/m², respectively.
 265 The corresponding values for downward shortwave radiative fluxes are 64 W/m², 97 W/m², 26 W/m².



266
 267
 268 Figure 7. The observed (dots) daily mean air temperature (a), snow depth (b), downward shortwave
 269 (c), and longwave (d) radiative fluxes for each ice season between 1 November and 31 May. The solid
 270 lines represent decadal daily maximum (red), minimum (green) and average (black) values. The
 271 shadow area represents the standard deviation (STD). For snow depth, daily mean values are given
 272 as thin color lines.

273
 274 Table 2 Summary of various meteorological and physical observations between 1 November and 31
 275 May. For meteorological parameters (*Va*, *Ta*, *RH*, *cn*, *Qs*, *Ql*) the values are seasonal mean ± standard
 276 deviation.

Season	<i>Va</i> m/s	<i>Ta</i> °C	<i>RH</i> (%)	<i>cn</i> (-)	<i>Qs</i> W/m ²	<i>Ql</i> W/m ²	<i>Tprec</i> (mm)	<i>Hsmax</i> (cm)	<i>AFDD</i> °C	<i>ATDD</i> °C
2009/2010	2.2±0.3	-6.8±9.4	84±9	0.7±0.1	62.9±76.8	267±31	201	101	-1717	304
2010/2011	2.2±0.6	-8±9.5	83±9	0.6±0.1	64.1±76.5	259±27	157	72	-1955	286
2011/2012	2.4±0.4	-5.1±7.2	84±11	0.7±0.1	64.4±82.3	264±21	272	91	-1308	239
2012/2013	2.2±0.2	-6.3±8.5	80±13	0.6±0.2	67±85.6	250±31	192	82	-1683	346

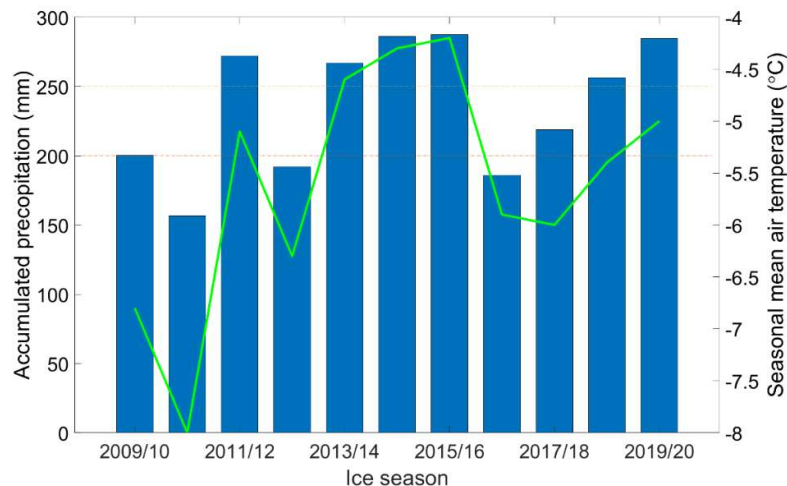
2013/2014	2.6±0.4	-4.6±6.4	81±10	0.7±0.1	61.6±81.8	261±19	267	81	-1214	243
2014/2015	2.7±0.6	-4.3±6.6	84±8	0.7±0.1	55.8±67.2	264±21	286	87	-1148	249
2015/2016	2.3±0.3	-4.2±8.4	84±10	0.7±0.1	61.5±81	265±25	287	106	-1261	354
2016/2017	2.8±0.3	-5.9±4.7	81±10	0.7±0.1	64.9±81.2	252±14	186	82	-1338	101
2017/2018	2.5±0.4	-6±8.7	80±12	0.7±0.2	66.5±82.7	256±27	219	101	-1615	362
2018/2019	2.7±0.4	-5.4±7.9	84±10	0.6±0.1	63.5±79.8	258±26	256	100	-1432	293
2019/2020	2.8±0.5	-5±5.1	84±13	0.6±0.1	70.1±92.9	258±13	285	124	-1242	188

277 *T_{prec}*: total accumulated precipitation in water equivalent (mm); *H_{smax}*: the maximum observed snow depth on land.

278 **AFDD: The accumulated freezing degree day**: the sum of daily mean air temperature below freezing point; **ATDD: The**
 279 **accumulated thawing degree day**: the sum of daily mean air temperature above freezing point.

280

281 Figure 7b clearly indicates that snow depth for the 2019/2020 season represented an extreme
 282 condition in a decade. There is an increasing trend of total precipitation during the ice season (Fig.
 283 8). The total seasonal accumulated total precipitation is highly correlated (correlation coefficient $r =$
 284 0.93) with the seasonal mean air temperature. The correlations between seasonal mean/maximum
 285 snow depth and corresponding air temperature are much lower $r = 0.40$ and $r = 0.38$, respectively.
 286 The correlation between total accumulated precipitation and maximum snow depth was 0.55. The
 287 difference is contributed by the snow drift and changes of snow metamorphism.



288

289 Figure 8. The accumulated total precipitation and mean air temperature between 1 November and 31
 290 May.

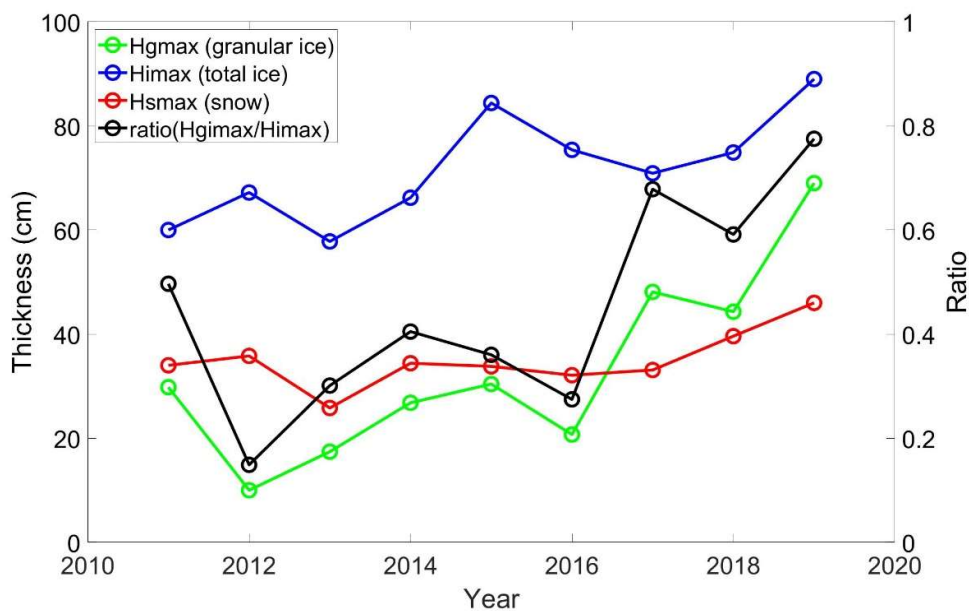
291

292

293 4. Discussions

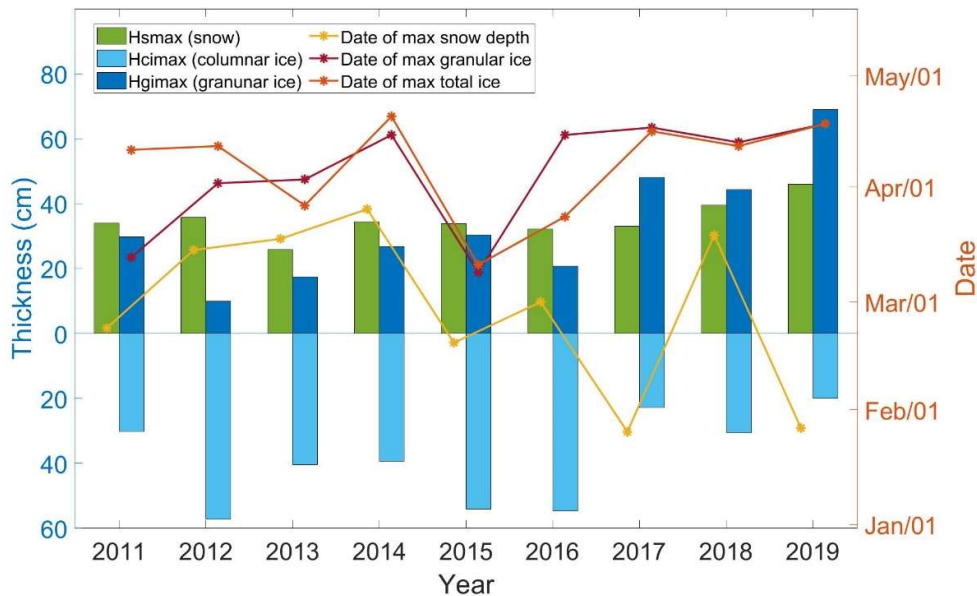
294 4.1 Inter-annual variation of SIMBA snow and ice products

295 Applying the SIMBA algorithm (Cheng et al., 2020), we obtained lake snow and ice products for all
296 seasons (see data availability). Figure 9 shows the observed seasonal maximum values for the snow
297 depth, maximum total ice thickness, and maximum granular ice thickness. During the observation
298 period, both snow depth and ice thickness showed increasing trends. The increase of granular ice
299 thickness is the fastest among all the snow and ice components. It reached the maximum 80% of the
300 total ice thickness in 2019/2020. In Lake Orajärvi, snow mass has contributed to the ice thickness
301 during every winter season. The maximum granular ice thickness was on average about 40% of the
302 maximum total ice thickness during the data period. For all seasons, the correlation coefficient
303 between the maximum granular ice thickness and the maximum ice thickness was 0.64. The
304 occurrence of maximum lake snow is, on the average, about one month prior to the maximum granular
305 ice formation (Fig. 10). Because of snow to ice transformation, the time series of snow depth in the
306 lake is not correlated with the snow depth on land. The snow depth on lake ice ranged from 25 to 43%
307 of that on land. On the average the ratio was 0.33, some 11% less than observed for a lake in southern
308 Finland (Kärkäs, 2000). In several seasons, when SIMBA were recovered in late April or early May,
309 the entire snow layer on lake ice was transferred to granular ice. Granular ice reached its maximum
310 value when the ice surface was free of snow.



311

312 Figure 9. SIMBA observed seasonal maximum snow depth (red), maximum total ice thickness (blue),
 313 maximum granular ice thickness (green) and the ratio between granular ice and total ice thickness
 314 (black) during observation seasons.



315
 316 Figure 10. Seasonal maximum snow depth, granular ice thicknesses, congelation ice thicknesses,
 317 and the date when those values were observed.

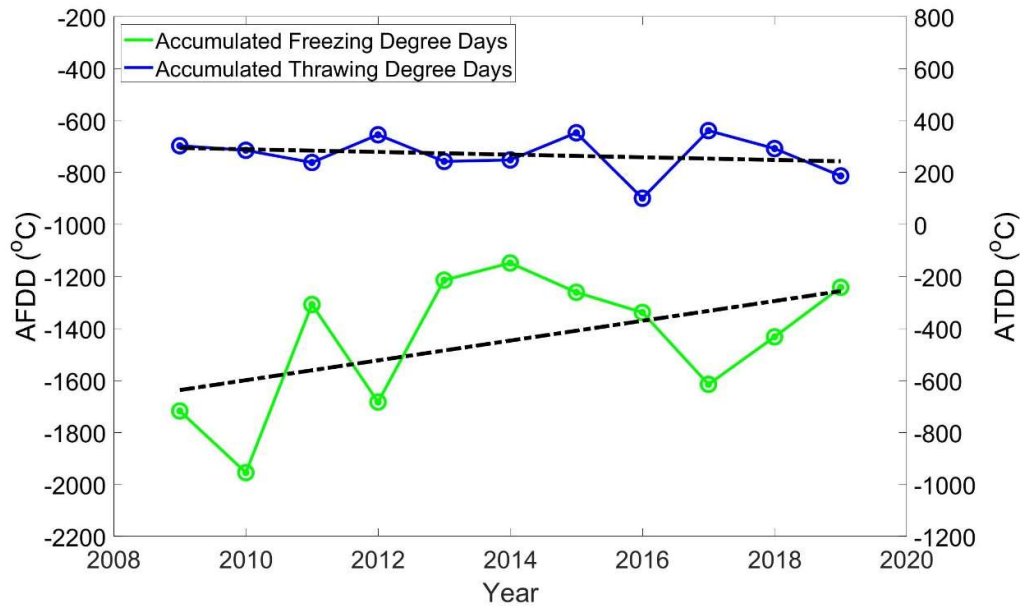
318

319 4.2 Inter-annual variation of temperature conditions

320 According to weather observations in Sodankylä, the air temperature increased by about 0.16 °C/year
 321 during the last decade. For the period from 1980 – 2020, the air temperature has an increasing trend
 322 of about 0.06 °C/year. On the average, the increase of air temperature in last decade is about 3 times
 323 faster than the past 40 years in agreement with the findings of Przybylak and Wszyński (2020) for
 324 the high Arctic. The accumulated precipitation correlated better to the maximum snow depth on land
 325 ($r = 0.55$) than the mean snow depth ($r = 0.45$). It is, however, not correlated ($r = 0.21$) with snow
 326 depth on the lake ice.

327 The seasonal AFDD and ATDD for each winter season are shown in Figure 11. A negative decreasing
 328 of AFDD was seen in response to the increase of air temperature. AFDD is directly linked with
 329 thermodynamic ice formation. During a given period, a decrease of AFDD is expected to result in
 330 less formation of columnar ice. However, during our observation period, the total ice thickness
 331 revealed an increasing trend. The increase of ice thickness is due to snow-ice formation. The trend of

332 ATDD is very insignificant, suggesting that the melting of lake ice due to temperature increase has
333 not increased much during the observation decade.



334
335 Figure 11. The seasonal accumulated freezing degree day (AFDD) and thaw degree day (ATDD)
336 during the observation period (2009/2010 – 2019/2020).
337

338 4.3 Challenges of the SIMBA program

339 SIMBA observations in Lake Orajärvi represent a small but sustainable program, so far ran for a
340 decade. A few times we have encountered malfunction of SIMBA, especially in the early phases of
341 the SIMBA program. In recent years, SIMBA has become more robust without need for heavy-duty
342 maintenances during field measurements, and the system has been remarkably improved with respect
343 to the quality of HT measurements. Several snow and ice products can be derived from SIMBA's two
344 type of temperature (SIMBA-ET and SIMBA-HT) measurements. The SIMBA program has largely
345 benefited from the Sodankylä supersite infrastructure, where the comprehensive and high standard
346 meteorological observations are available.

347 Challenges remain in further improvement of the SIMBA program. Due to safety issues, SIMBA must
348 be deployed and recovered when ice is strong enough. Hence, the early freeze-up and late break-up
349 cannot be monitored. In Autumn 2019, a wooden floating raft was deployed and anchored in Lake
350 Orajärvi. SIMBA was, for the first time, deployed during ice-free season on 1 October. This kind of
351 deployment will be carried out also in the future, allowing year-round SIMBA measurements.

352 Part of the thermistor chain exposed in the air above the snow surface may suffer from frost in winter
353 or from solar heating in spring, and also the sensors in the upper layers of snow and ice may suffer
354 from solar heating, resulting in large uncertainties in SIMBA-ET and SIMBA-HT readings. To
355 compensate the effect of temperature errors on snow depth detection, one solution is to deploy
356 Acoustic Rangefinder Sounders (ARS) to measure the evolution of snow surface. In fact, an ARS has
357 been deployed in the past two winter seasons. These data sets can also be used to understand the effect
358 of wind on snow drift and quantify snow surface sublimation in winter.

359 During the melting season, both SIMBA-ET and SIMBA-HT strongly raise in the upper part of the
360 ice resulting an isothermal status of the entire ice column. In this condition, SIMBA snow depth and
361 ice thickness values are liable to large errors. Combination of SIMBA observations and numerical
362 model experiments may yield more reliable results in such conditions.

363 SIMBA measurements have been taken automatically, but it is still important to carry out manual on
364 site observations, such as collecting ice core and snow samples, as such observations cannot be made
365 by automatic instruments.

366

367 **4 Data availability**

368 The data are archived at <https://zenodo.org/record/4559368#.YEIYOtyxVPZ> (Cheng et al., 2021).

369 The 4 zip-files should be unzipped in different file folders preferably using zip-file names as the
370 folder names. A readme file exists in each folder. The manual in situ snow depth and ice thickness
371 observation for 2009/2010 - 2012/2013 as well as a description of SIMBA deployment and recovery
372 for each ice season (SIMBA_D&R_all_Years.docx) are provided.

373

374 **5 Conclusions**

375 A thermistor string-based snow and ice mass balance apparatus (SIMBA) has been deployed in an
376 Arctic lake since 2009. The measurements covered most part of the ice season from mid-December
377 to late April/early May. SIMBA-ET and SIMBA-HT temperature observations are described in this
378 paper. The daily snow depth and ice thickness were derived from SIMBA temperature field applying
379 a validated automatic algorithm (Cheng et al., 2020). The meteorological parameters for winter
380 seasons (1 November - 31 May) are also collected and discussed. During the investigation decade,
381 the air temperature in the ice season has had an increasing trend of 0.16 °C/year. The warming rate is

382 comparable to the result find for the high Arctic by Przybylak and Wyszyński (2020). The increase of
383 air temperature in winter season is highly correlated (0.93) with seasonal total accumulated
384 precipitation. This is because warm winters in the study region are also wet and characterized by a
385 high cyclone activity. Transient cyclones are vital for the transport of warm, moist air masses to
386 Northern Europe (Wickström et al., 2020). The precipitation in season 2019/2020 represented an
387 extreme episode during the study decade. Despite of the air temperature increase, the total maximum
388 ice thickness in the lake has an increasing trend. The increase of maximum ice thickness is due to the
389 increase of granular ice. The interannual variability of maximum granular ice thickness is large
390 ranging from 15 to 80% of the total maximum ice thickness. The time series of the SIMBA ET and
391 HT allow identification of moving air-snow, snow-ice and ice-water interfaces. Because of the air
392 temperature increase, the seasonal AFDD reduces. This results in a decreasing impact of below-zero
393 air temperatures on lake ice growth during the freezing season, as the growth of columnar ice is
394 reduced. Simultaneously, the role of precipitation on total ice formation is enhanced because snow-
395 ice and superimposed ice contribute to an increasing fraction of the total ice thickness. The trend in
396 ATDD was negligible, suggesting that the effect of air temperature on ice melting has remained
397 unchanged.

398 To our knowledge, this is the first decadal-scale SIMBA data set ever collected from an Arctic lake.
399 The data provides information on snow and ice mass balance and the controlling atmospheric factors.
400 The measurements will continue in the future.

401 The weather observations, e.g. decadal time series of daily maximum and minimum weather
402 parameters, can be used to estimate snow and ice conditions in the lake applying a snow/ice model
403 (e.g. Cheng et al., 2014). The SIMBA data are not only suitable for snow/ice surface heat and mass
404 balance studies. The temperatures at the ice bottom and in the water below are valuable to understand
405 the lake thermal structure and water-ice heat transfer (Huang et al., 2019b).

406 The SIMBA program, with Lake Orajärvi as a testbed, offers excellent opportunities for
407 dissemination of cryospheric knowledge and related outreach, providing rich possibilities for
408 community collaborations both nationally and internationally. The observed changes in snow depth
409 and composition of lake ice contribute to better understanding of cryospheric aspects of climate
410 change. For example, parameterizations of the discovered snow and ice processes can be improved
411 in climate models.

412 Snow and ice measurements similar to those in Lake Orajärvi have been recently initiated in
413 Wulaingsuhai lake in an arid climate zone in Inner-Mongolia of China. The observations focused on
414 lake ice mass balance (Lu et al., 2020) and energy budget, in particular the solar radiation (Cao et al.,
415 2020). In a long run, the corresponding lake snow and ice measurements at both sites and possible
416 similar observations in a thermokarst lake (e.g. Huang et al, 2019a, 2019b) at Qinghai-Tibet Plateau,
417 often referred to as the “Third Pole of the Earth” can be used together to carry out coordinated research.
418

419 **Acknowledgement**

420 We are grateful to Mr. Pekka Kosloff for carrying out fieldwork in Lake Orajärvi for all the winter
421 seasons. The logistical assistance provided by Mr. Jyrki Mattanen in FMI-ARC, Sodankylä are
422 acknowledged. The study was for financial support by FMI long-term sustainable SIMBA program.
423 The data analyses were partly supported by the European Union’s Horizon 2020 research and
424 innovation programme [727890 – INTAROS]; Academy of Finland under contract 317999, and the
425 National Key Research and Development Program of China (No. 2017YFE0111700 – MARIS)

426

427

428 **References**

429 Anderson, E.J., Fujisaki-Manome, A., Kessler, J., Lang, G.A., Chu, P. Y., Kelley, J.G.W., Chen, Y.,
430 and Wang, J.: Ice Forecasting in the Next-Generation Great Lakes Operational Forecast System
431 (GLOFS), *J. Mar. Sci. Eng.*, 6, 123; doi:10.3390/jmse6040123, 2018.

432 Ballinger, T.J., Overland, J.W., Wang, M., Bhatt, U.S., Hanna, E., Hanssen-Bauer, I., Kim, S.-J.,
433 Thoman, R.L., and Walsh, J.E.: Surface air temperature, Arctic Report Card, [DOI: 10.25923/gcw8-
434 2z06](https://doi.org/10.25923/gcw8-2z06), 2020.

435 Bintanja, R.: The impact of Arctic warming on increased rainfall, Scientific Report.
436 DOI:10.1038/s41598-018-34450-3, 2018.

437 Box, J.E. and 19 others: Key indicators of Arctic climate change: 1971–2017, *Environ. Res. Lett.* 14
438 045010, 2019.

439 Brown, L. C. and Duguay, C.R.: The response and role of ice cover in lake climate interactions.
440 *Progress in Physical Geography: Earth and Environment* 34(5), 671–704, 2010.

441 Cheng, B., Vihma T., Rontu, L., Kontu, A. Kheyrollah Pour H., Duguay C. and Pulliainen, J.:

442 Evolution of snow and ice temperature, thickness and energy balance in Lake Orajärvi, northern
443 Finland, *Tellus A: Dynamic Meteorology and Oceanography* 66(1), 21564, 2014.

444 Cheng, Y., Cheng, B., Zheng, F., Vihma, T., Kontu, A., Yang, Q. and Liao, Z.: Air/snow, snow/ice and
445 ice/water interfaces detection from high-resolution vertical temperature profiles measured by ice
446 mass-balance buoys on an Arctic lake, *Annals of Glaciology* 1–11. [https://doi.org/10.1017/
447 aog.2020.51](https://doi.org/10.1017/aog.2020.51), 2020

448 Cheng, B., Cheng, Y., Vihma, T., Kontu, A., Zheng, F., Lemmetyinen, J., and Pulliainen, J.: SIMBA
449 snow/ice mass balance buoy data and weather station data[Data set]. *Earth System Science Data*
450 (ESSD). Zenodo. <http://doi.org/10.5281/zenodo.4559368>, 2021.

451 Cao, X., Lu, P., Leppäranta, M., Arvola, L., Huotari, J., Shi, X., Li, G., and Li, Z.: Solar radiation
452 transfer for an ice-covered lake in the central Asian arid climate zone. *Inland Waters*,
453 doi:10.1080/20442041.2020.1790274, 2020.

454 Filazzola, A., Brown, C., Dettlaff, M.A., Batbaatar, A., Grenke, J., Bao, T., Heida, I.P., and Cahill
455 Jr, J.F.: The effects of livestock grazing on biodiversity are multitrophic: a meta-analysis, *Ecology*
456 *Letters*, 23: 1298–1309, <https://publons.com/publon/10.1111/ele.13527>, 2020.

457 Hoppmann, M., Nicolaus, M., Hunkeler, P. A., Heil, H., Behrens, L.-K. König-Langlo, G., and Gerdes,
458 R.: Seasonal evolution of an ice-shelf influenced fast-ice regime, derived from an autonomous
459 thermistor chain, *J. Geophys. Res. Oceans*, 120, 1703–1724, doi:10.1002/2014JC010327, 2015.

460 Huang, W., Cheng, B., Zhang, J., Zhang, Z., Vihma, T., Li, Z., and Niu, F.: Modeling experiments on
461 seasonal lake ice mass and energy balance in the Qinghai–Tibet Plateau: a case study, *Hydrol. Earth*
462 *Syst. Sci.*, 23, 2173–2186, <https://doi.org/10.5194/hess-23-2173-2019>, 2019a.

463 Huang, W., Zhang, J., Leppäranta, M., Li, Z., Cheng, B. and Lin, Z.: Thermal structure and water-ice
464 heat transfer in a shallow ice-covered thermokarst lake in central Qinghai-Tibet Plateau. *Journal of*
465 *Hydrology*, 578, [124122]. <https://doi.org/10.1016/j.jhydrol.2019.124122>, 2019b

466 Jackson, K., Wilkinson, J., Maksym, T., Meldrum, D., Beckers, J., Haas, C., and Mackenzie, D.: A
467 novel and low-cost sea ice mass balance 1010 buoy. *J. Atmos. Ocean. Tech.* 30(11), 2676–2688. DOI:
468 10.1175/JTECH-D-13-00058.1., 2013

469 Kang, K.-K., Duguay, C.R., Lemmetyinen, J., and Gel, Y.: Estimation of ice thickness on large
470 northern lakes from AMSR-E brightness temperature measurements. *Remote Sensing of*
471 *Environment* 150, 1–19, doi: 10.1016/j.rse.2014.04.016, 2014.

472 Kärkäs, E-: The ice season of Lake Pääjärvi in southern Finland. *Geophysical Research Letters* 36(1–
473 2), 85–94, 2000.

474 Lei, R., Cheng, B., Heil, P., Vihma, T., Wang, J., Ji, Q., and Zhang, Z.: Seasonal and interannual
475 variations of sea ice mass balance from the central Arctic to the Greenland Sea. *Journal of*
476 *Geophysical Research: Oceans* 123(4), 2422–2439, 2018.

477 Lei, R., Hoppmann, M., Cheng, B., Zuo, G., Gui, D., Cai, Q., Belter, H. J., and Yang, W.: Seasonal
478 changes in sea ice kinematics and deformation in the Pacific sector of the Arctic Ocean in 2018/19,
479 *The Cryosphere*, 15, 1321–1341, <https://doi.org/10.5194/tc-15-1321-2021>, 2021.

480 Leppäranta, M.: Modelling the formation and decay of lake ice. In George G (ed.), *The Impact of*
481 *Climate Change on European Lakes*. Dordrecht, Netherlands: Springer, pp. 63–83, 2010.

482 Leppäranta, M.: *Freezing of Lakes and the Evolution of Their Ice Cover*. Berlin Heidelberg: Springer,
483 2015.

484 Liao, Z., Cheng, B., Zhao, J., Vihma, T., Jackson, K., Yang, Q., Yang, Y., Zhang, L., Li, Z. Qiu, Y. and
485 Cheng, X.: Snow depth and ice thickness derived from SIMBA ice mass balance buoy data using an
486 automated algorithm. *International Journal of Digital Earth* 12(8), 962–979, 2019.

487 Lu, P., Cao, X., Li, G., Huang, W., Leppäranta, M., Arvola, L., Huotari, J., and Li, Z.: Mass and heat
488 balance of a lake ice cover in the central Asian arid climate zone. *Water*, 12(10), 2888,
489 [doi:10.3390/w12102888](https://doi.org/10.3390/w12102888), 2020.

490 Mermoz, S., Allain-Bailhache, S., Bernier, M., Pottier, E., Sanden, J. J. Van Der, and Chokman. K.:
491 Retrieval of river ice thickness from C-band PolSAR data. *IEEE Transactions on Geoscience and*
492 *Remote Sensing* 99, 1–11, [doi: 10.1109/TGRS.2013.2269014](https://doi.org/10.1109/TGRS.2013.2269014), 2013.

493 Provost, C., Sennechaël, N., Miguet, J., Itkin, P., Rosel, A., Koenig, Z., Villaceros-Robineau, N., and
494 Granskog. M.A.: Observations of flooding and snow-ice formation in a thinner Arctic sea-ice regime
495 during the N-ICE2015 campaign: influence of basal ice melt and storms. *Journal of Geophysical*
496 *Research: Oceans* 122(9), 7115–7134, [doi:10.1002/2016JC012011](https://doi.org/10.1002/2016JC012011), 2017.

497 Przybylak R, Wyszynski P.: Air temperature changes in the Arctic in the period 1951– 2015 in the
498 light of observational and reanalysis data. *Theor. Appl. Climatol.* 139: (1–2):75–94.
499 DOI: [10.1007/s00704-019-02952-3](https://doi.org/10.1007/s00704-019-02952-3), 2020

500 Richter-Menge JA, Perovich DK, Elder BC and Claffey K: Ice mass balance buoys: a tool for
501 measuring and attributing changes in the thickness of the Arctic sea-ice cover. *Annals of Glaciology*

502 44, 205–210. 2006

503 Sharma, S., Blagrove, K., Magnuson, J.J., M. O'Reilly, C., Oliver, S., D. Batt, R., R. Magee, M.,
504 Straile, D., Weyhenmeyer, G.A. Winslow, L., Woolway, R.I.: Widespread loss of lake ice around the
505 Northern Hemisphere in a warming world. *Nat. Clim. Chang.* 9, 227–231.
506 <https://doi.org/10.1038/s41558-018-0393-5>, 2019.

507 Tikkanen, M.: Climate. In: *The Physical Geography of Fennoscandia* (ed. M. Seppälä). Oxford:
508 Oxford University Press, pp. 96112, 2005.

509 Wei L., Deng X., Cheng B., Vihma T., Hannula H., Qin T., and Pulliainen J.: The impact of
510 meteorological conditions on snow and ice thickness in an Arctic lake. *Tellus - Series A: Dynamic
511 Meteorology and Oceanography*, Vol 68: 1–12, 2016.

512 Wickström, S., Jonassen, M., Vihma, T., and Uotila, P.: Trends in cyclones in the high latitude North
513 Atlantic during 1979–2016. *Q. J. R. Meteorol. Soc.*, 146, 762–779, DOI: 10.1002/qj.3707, 2020.

514 Woolway, R., Weyhenmeyer, G.A., Schmid, Dokulil, M.T., de Eyto, E., Maberly, S.C., May, L., and
515 Merchant, C. J.: Substantial increase in minimum lake surface temperatures under climate change.
516 *Climatic Change* 155, 81–94. <https://doi.org/10.1007/s10584-019-02465-y>, 2019.

517 Wu, Y., Duguay, C, R, and Xu, L.: Assessment of machine learning classifiers for global lake ice
518 cover mapping from MODIS TOA reflectance data, *Remote Sensing of Environment*, Vol 253,
519 112206 <https://doi.org/10.1016/j.rse.2020.112206>, 2021.

520 Zuo, G., Dou, Y., Lei, R.: Discrimination algorithm and procedure of snow depth and sea ice thickness
521 determination using measurements of the vertical ice temperature profile by the ice-tethered buoys.
522 *Sensors* 18, 4162. <https://doi.org/10.3390/s1812416>, 2018.

523

524

525